Available online at www.sciencedirect.com
ScienceDirect
Ceramics International 35 (2009) 2907–2913
CERAMICS INTERNATIONAL
www.elsevier.com/locate/ceramint

Mechanical and fracture properties of zircon–mullite composites obtained by direct sintering

N.M. Rendtorff [a,b,*], L.B. Garrido [a], E.F. Aglietti [a,b]

[a] Centro de Tecnología de Recursos Minerales y Cerámica (CETMIC) (CIC-CONICET-CCT La Plata), Camino Centenario y 506, C.C. 49 (B1897ZCA) M.B. Gonnet, Buenos Aires, Argentina
[b] Facultad de Ciencias Exactas, Universidad Nacional de La Plata, UNLP, Argentina

Received 27 January 2009; received in revised form 23 February 2009; accepted 29 March 2009
Available online 24 April 2009

Abstract

Refractory materials based on zircon ($ZrSiO_4$) are applied in high temperature applications (1400–1500 °C). They are demonstrated to have an excellent chemical attack resistance, such as corrosion or degradation due to molten glass or metals. On the other hand mullite ($3Al_2O_3 \cdot 2SiO_2$) is important both in traditional and advanced ceramics. Although multi-phase ceramic materials were always used, nowadays composite materials have an important industrial and technological development, to enlarge the designing capability of the manufacturer in properties and behaviors. The objective of the present work is to study the influence of the starting composition on the mechanical and fracture properties of zircon–mullite composites obtained by direct sintering of consolidated samples by slip cast of concentrated aqueous suspensions in plaster molds. Zircon–mullite composites using 15–45 wt% mullite were prepared and compared with pure zircon material obtained in the same conditions. Flexural strength (σ_f), dynamic elastic modulus (E), toughness (K_{IC}) and initiation fracture surface energy (γ_{NBT}) were evaluated. The results were explained by microstructure and the XRD analysis. The presence of mullite increased the zircon thermal dissociation. The ZrO_2 was a product of this reaction and also influence the mechanical and fracture properties of these materials through several combined mechanisms.

Zircon composites prepared with 45 wt% of mullite in the starting powder showed a higher fracture toughness and initiation energy than ceramics derived from pure zircon. Microstructure consisting in mullite as a continuous predominant phase in which zircon and zirconia grains were distributed improved almost all the mechanical and fracture properties.

Keywords: C. Mechanical properties; C. Fracture properties; D. Mullite; Zircon

1. Introduction

Nowadays composite materials have an important industrial and technological development. The designing capability of the manufacturer in properties and behaviors is enhanced by combining two or more different materials however the final properties do not necessarily be between the pure material ones. Once the constituent phases and the processing conditions are chosen the phase proportion becomes one of the most important processing variables.

Zircon ($ZrSiO_4$) is a good refractory material because it does not undergo any structural transformation until its dissociation at about 1450–1700 °C, depending on the present impurities. It exhibits many attractive properties such as excellent chemical stability coupled with a very low thermal expansion coefficient (4.1×10^{-6} °C^{-1}) from room temperature to 1400 °C and low heat conductivity coefficient (5.1 W/m °C at room temperature and 3.5 W/m °C at 1000 °C). Sintered zircon with high purity can retain its bending strength up to temperatures of 1200 and 1400 °C [1]. These properties make zircon a useful structural ceramic. These materials are widely utilized in the glass industries [2–4]. The presence of impurities decreases the dissociation and usage temperatures.

The mullite ceramics has had and will continue to have a significant role in the development of traditional and advanced ceramics [5–7]. Mullite is the only stable crystalline phase in

* Corresponding author at: Centro de Tecnología de Recursos Minerales y Cerámica (CETMIC) (CIC-CONICET-CCT La Plata), Camino Centenario y 506, C.C. 49 (B1897ZCA) M.B. Gonnet, Buenos Aires, Argentina.
Tel.: +54 2214840247; fax: +54 2214710075.
E-mail address: rendtorff@hotmail.com (N.M. Rendtorff).

0272-8842/$36.00
doi:10.1016/j.ceramint.2009.03.040

the aluminosilicate system, under normal atmospheric pressure from room to elevated temperatures [6]. Its chemical composition ranges from $3Al_2O_3$–$2SiO_2$ to approximately $2Al_2O_3$–SiO_2. It has received significant attention during the last decades as a potential structural material for high temperature applications [7].

Zircon based ceramics have been processed by, room temperature and hot pressing, sol–gel and slip casting [8–11]. Zircon materials sintered in the range between 1500 °C and 1650 °C achieved densities over the 99% of the theoretical depending on the processing route. There are several studies of composites with zircon as the principal phase [12–15], and more than a few studies of composites with mullite [5–7]. Zircon–mullite material obtained by reaction sintering has been recently studied [14]. Although zircon and mullite are different from the chemical and crystallographic point of view, their mechanical properties are similar.

In this study zircon composites containing up to 45 wt% of mullite were prepared by slip casting of concentrated aqueous suspensions. The influence of the different phase content and distribution was examined and compared with that of a pure zircon ceramic. A microstructural, structural, mechanical and fracture characterization of the composites was carried out.

2. Experimental

2.1. Slip casting of dense zircon–mullite composite

A commercial zircon ($ZrSiO_4$) powder was used as principal raw material, with ZrO_2 = 64–65.5 wt%, SiO_2 = 33–34 wt%, $Fe_2O_3 \leq 0.10$ wt% and $TiO_2 \leq 0.15$ wt%, mean diameter (D_{50}) of 1.5 μm, specific gravity of 4.6 g/cm^3, melting point of 2200 °C and hardness (Mohs) of 7.5 (Kreutzonit Super, Mahlwerke Kreutz, Germany).

A commercial mullite powder was used as the second raw material, with mullite 90–95 wt%, glassy phase 5–10%, apparent density of 2.80 g/cm^3, true density of 3.13 g/cm^3, Al_2O_3 = 72%, SiO_2 = 20%, Fe_2O_3 = 0.2%, CaO–MgO = 0.3%, K_2O–Na_2O = 0.5%, mean diameter (D_{50}) of 2 μm (Synthetic mullite M72, VAW, Veremigte, Werke AG, Germany).

Zircon and mullite mixtures were prepared with 15, 25, 35 and 45 wt% of mullite and were called ZM15, ZM25, ZM35 and ZM45 respectively. The pure zircon material was named Z0.

The processing route chosen had been explained in a previous work [15]. Aqueous 80 wt% suspensions of the mixtures at pH 9.1–9.2 were prepared by adding the powder to aqueous solutions with suitable content of dispersant (Dolapix CE64, Zschimmers and Schwartz) and NH_4OH. After mixing, the suspensions were ultrasonicated for 20 min. The prismatic bars 7.5 mm × 7.5 mm × 50 mm were produced from well dispersed suspensions by slip casting in a plaster molds. Dried probes were fired in an electric furnace with a heating rate of 10 °C/min up to 1600 °C for 2 h.

2.2. Characterization techniques

Density and open porosity of sintered samples were determined by the water absorption method. Crystalline phases formed were analyzed by X-ray diffraction (XRD) (Philips 3020 equipment with Cu-Kα radiation in Ni filter at 40 kV–20 mA). The Rietveld method [16,17], a quantitative analysis, was carried out to characterize the present crystalline phases in the materials. The XRD patterns were analyzed with the program FullProf, which is a multipurpose profile-fitting program, including Rietveld refinement [18]. Theoretical density was calculated taking into account the density of each component: 3.13 g/cm^3 for mullite, 4.56 g/cm^3 for zircon and 5.89 g/cm^3 for zirconia considering the final crystalline phases evaluated by the Rietveld method. The dynamic elastic modulus E of the composites was measured by the excitation technique with a GrindoSonic, MK5 ''Industrial'' Model. A theoretical estimation of the elastic modulus (E_{teo}) was made; this was defined by the following expression:

$$E_{teo} = \sum (E_i V_i) \quad (1)$$

where E_i and V_i are the elastic modulus and the volume fraction of each crystalline phase defined before. The values for each phase elastic modulus were (244 MPa, 204 MPa and 200 MPa for zircon, mullite and m-ZrO_2 respectively).

Microstructural examination was conducted with a scanning electron microscope (SEM) (Quanta 200 MK2 Series de FEI) after polishing the probes surface until to 1 μm diamond paste. Flexural strength (σ_f) was measured on the bars with rectangular section using the three-point bending test with a span of 40 mm and a displacement rate of 2.5 mm/min was employed (Universal testing machine INSTRON 4483). The fracture intensity factor (K_{IC}) and the fracture initiation energy (γ_{NBT}) were evaluated by the single edge notched beam (SENB) method [19,20] using a three-point bending universal testing machine. Samples of dimensions (7.5 mm × 7.5 mm × 50 mm) were notched with diamond saw of 0.3 mm thickness, with depth between 0.3 mm and 2.5 mm. The three-point test was carried out at room temperature with a displacement rate of 0.1 mm/min. In this method K_{IC} is given by

$$K_{IC} = \frac{3QLC^{1/2}}{2WD^2} \times \left[A_0 + A_1\left(\frac{C}{D}\right) + A_2\left(\frac{C}{D}\right)^2 + A_3\left(\frac{C}{D}\right)^3 + A_4\left(\frac{C}{D}\right)^4 \right] \quad (2)$$

where Q is the load applied to the notched bar, L is the span, C is the depth of the notch, D is the thickness of the specimen, W is the width of the specimen, and A0, A1, A2, A3 and A4 are functions of the ratio (L/D) described in [19,20].

The calculated values of K_{IC}, together with E, were used to estimate the initiation fracture energy for the area created by the crack propagation (γ_{NBT}) evaluated by the SENB test, using the subsequent equation [19,20]:

$$K_{IC} = \sqrt{2\gamma_{NBT}E} \quad (3)$$

where γ_{NBT} can be expressed as

$$\gamma_{NBT} = \frac{K_{IC}^2}{2E} \quad (4)$$

3. Results and discussion

3.1. Density

The textural characterization of the materials is shown in Table 1, all the materials processed showed a very low open porosity. All the composite materials showed a similar densification (92%), higher than for the pure zircon material. Therefore some closed porosity existed and glassy phase is expected to occur in the grain boundaries.

3.2. Crystalline phases

Diffractograms of the materials are shown in Fig. 1. The major phases in the composite were zircon and mullite labeled with *z* and *m* respectively except for Z0 where the major phase is only zircon. Small reflections of Baddeleyite (*m*-ZrO_2) and *t*-ZrO_2 can be observed in Fig. 2, which is a detail of the previous XRD pattern. ZrO_2 is a product of the thermal dissociation of the zircon. The temperature at which this reaction starts depends on the presence of impurities and other phases [21]. Zirconia undergoes martensitic transformation from monoclinic to tetragonal phase at around 1100 °C in a heating step and the inverse transformation during cooling occurs around 900 °C, but it has been stated that if the grain is smaller than a critical size the tetragonal phase is retained. So particularly the presence of the tetragonal zirconia phase indicated the existence of zirconia particles smaller than its critical size, consequently the inverse transformation occurred partially. Although *t*-ZrO_2 grains can improve toughness through the transformation toughening, the proportion of *t*-ZrO_2 is low compared to *m*-ZrO_2 (Table 2). So the toughness improvement is probably more linked to the total amount of zirconia and can be due to a microcraking mechanism.

In Fig. 2 the increase in the amount of three minor phases: mullite, *m*-ZrO_2 and *t*-ZrO_2 is clearly observed. The initial raw material proportions and the final crystalline composition of the materials studied are shown in Table 2. The final amount of each crystalline phase was evaluated by the Rietveld method. Since the quantity of zircon decreased in this series it is evident that the high content of mullite increased the decomposition of zircon. The *t*-ZrO_2 was in all the cases around 7% of all the zirconia present in the composite. Then retention of this phase was not influenced by the change in the initial composition. Also the size of these grains and local stiffness of the ceramic matrix are similar in all the composites studied.

Table 3 shows the final composition expressed as volume percentage. Due to the low density of mullite compared to the other phases (3.13 g/cm^3 for mullite, 4.56 g/cm^3 for zircon and 5.89 for zirconia) its volume content was higher than that in the weight composition.

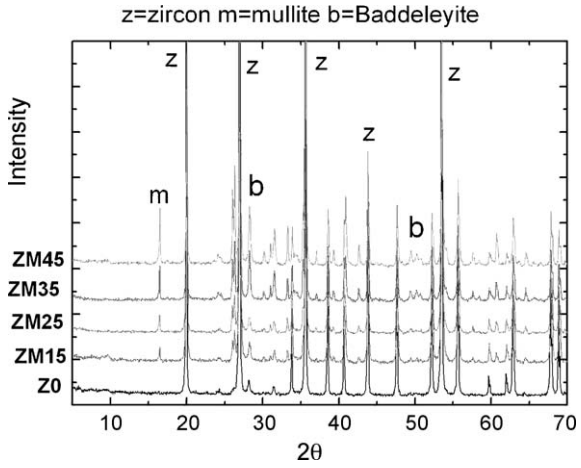

Fig. 1. XRD, diffractograms of the studied materials.

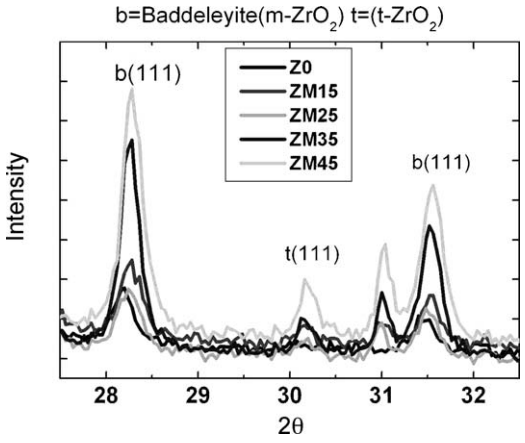

Fig. 2. XRD, diffractograms of the studied materials (detail).

Table 1
Texture properties of the studied materials.

	Apparent density (g/cm^3)	$\rho_{Theoretical}$ (%)	Open porosity (%)
Z0	4.10	88	1
ZM15	3.99	92	<1
ZM25	3.85	92	<1
ZM35	3.70	92	<1
ZM45	3.55	92	≈1

Table 2
Initial and final compositions of the studied materials.

Sample	Initial composition (wt%)		Final crystalline phases (wt%)			
	Zircon	Mullite	Zircon	Mullite	*m*-ZrO_2	*t*-ZrO_2
Z0	100	0	96.5	0	3.5	0.17
ZM15	85	15	82	14	4	0.29
ZM25	75	25	73	23	4	0.35
ZM35	65	35	54	34	11	0.65
ZM45	55	45	46	44	10	0.75

Table 3
Volume fraction of the studied materials.

	Final crystalline phases (vol%)		
	Zircon	Mullite	Zirconia
Z0	97.0	0.0	3.0
ZM15	79.8	16.7	3.5
ZM25	69.6	27.0	3.4
ZM35	51.2	39.6	9.2
ZM45	42.2	49.6	8.2

All the materials showed a relatively dense packing taking into account that they were processed by slip casting from good aqueous dispersion with high solid content.

3.3. Microstructure

SEM micrographs of the Z0, ZM15, ZM35 and ZM45 materials are shown in Figs. 3–6 respectively. All the samples had a dense microstructure with low residual porosity (P). There is no preferential direction or orientation of the mullite grains in the microstructures of these materials. These are similar to the one obtained by different processing methods [8–11,14]. The images demonstrate that a high sintering was achieved for all the composites. However the sinterization process of the pure zircon material (Z0; Fig. 3) shown to be in the final stage of the sintering with large necking and closed voids of relatively large size remaining in the matrix, in concordance with the densification results shown in Table 1. In Fig. 3, the principal crystalline phase observed in Z0 is $ZrSiO_4$ (labeled with a Z). As some diffraction lines of *m*-ZrO_2 and *t*-ZrO_2 were observed for the pure zircon material (Fig. 2) some zirconia grains can be observed detected with EDAX (labeled with B). The darker zones in the micrograph (labeled with P) are closed pores.

Processed in the same conditions, composite materials (ZM15-45) show a higher sinterization grade with a lower porosity (P). Different crystalline phases were observed and characterized by EDAX: dark gray grains of mullite (M), middle gray grains of zircon (z). In all the cases rounded zirconia white grains can be observed (B) product of the thermal decomposition of zircon. These are associated or near the zircon grains and the zircon–mullite interface.

ZM15 and ZM25 composites reveal a phase configuration formed with a zircon matrix and well dispersed mullite (10–15 μm) and zirconia (1–2 μm) grains (Fig. 4). The initial mean diameter of the starting mullite powder was five times smaller than the grains in the sintered material showing a grain growth process.

Considering the volume fraction of the three principal phases (Table 3), it is clear that in ZM45 a change in the microstructure appears (Fig. 6). In this material mullite is the

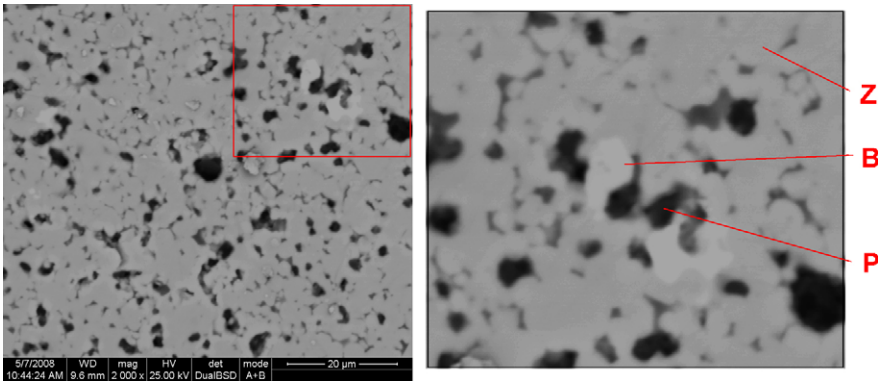

Fig. 3. SEM micrograph of the Z0 material.

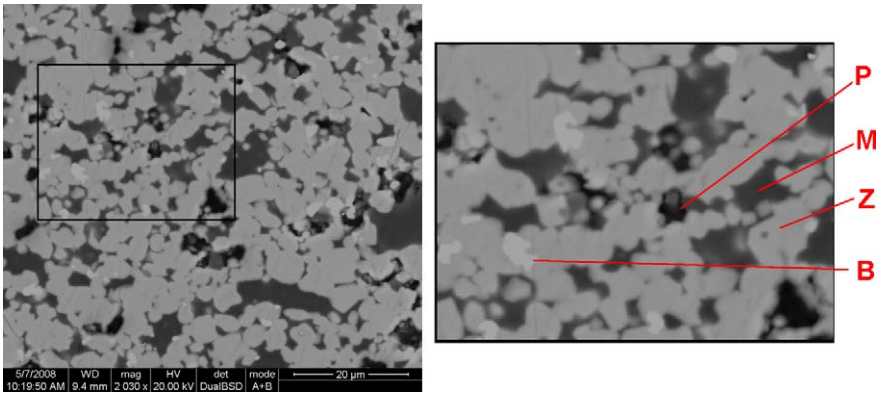

Fig. 4. SEM micrograph of the ZM15 material.

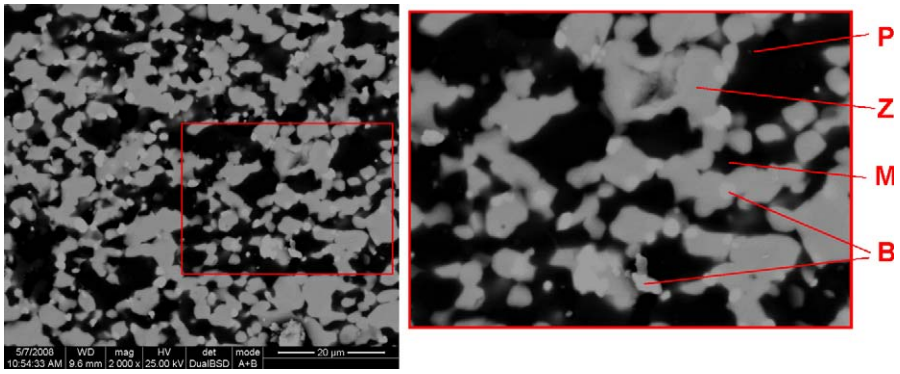

Fig. 5. SEM micrograph of the ZM35 material.

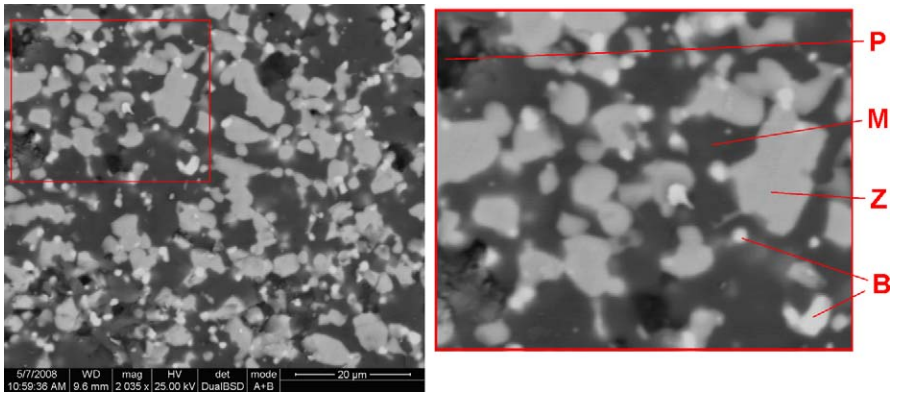

Fig. 6. SEM micrograph of the ZM45 material.

continuous phase and acts as a matrix for zircon and zirconia grains. In this sample zircon grains show a grain size minor to 10 μm and zirconia grains appear as dispersed grains smaller than 2 μm. The zircon initial mean diameter was around 2 μm evidencing a grain growth process during sintering.

The microstructure of the ZM35 material (Fig. 5) appeared as intermediate between the other two configurations showing the difficulty to determine which component acts as matrix.

3.4. Elastic modulus (E0) and flexural strength (σ_f)

The impulse excitation technique was used to evaluate the elastic modulus. The results obtained by this method are reliable and comparable data with those obtained by other methods such as three- and four-point bending methods or indentation techniques [24].

The experimental elastic modules of the composites as a function of the mullite content are shown in Fig. 7. The values obtained are slightly lower than that of pure zircon and pure mullite ceramics (244 GPa and 204 GPa respectively) [14]. Residual porosity of the composites was probably the main cause of the low measured modulus in comparison with the two single component materials.

In Fig. 7, a theoretical elastic modulus estimation (E_{teo}) is plotted against the amount of mullite. Both experimental and theoretical elastic modulus of these materials decreased almost linearly with the increasing mullite content. This behavior is clearly shown in Fig. 7. The fitted straight lines follow the equations:

$$E_{teo} = 243 - 0.51M \quad (5)$$

$$E = 213 - 0.92M \quad (6)$$

where M is the mullite wt% incorporated in the composite and E_{teo} and E are the values of the theoretical and dynamic elastic modulus in GPa.

The higher slope (absolute value) of the experimental equation shows that the experimental change is higher than the change expected only taking into account the volume phase content of each phase and its contribution to the elasticity of

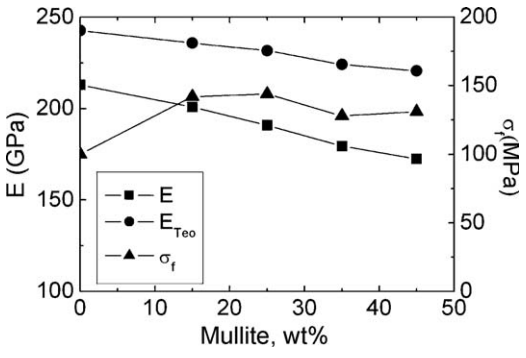

Fig. 7. Dynamic elastic modulus and flexural strength of the studied materials.

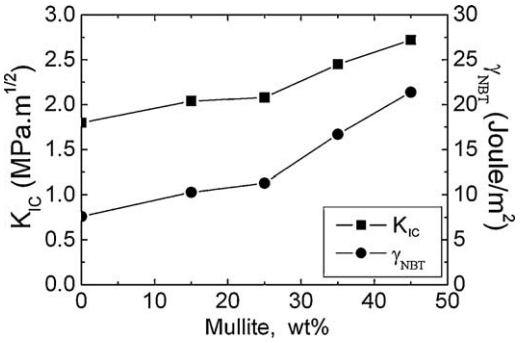

Fig. 8. Fracture toughness K_{IC} and initiation surface energy γ_{NBT} as functions of the amount of mullite powder in the initial composition.

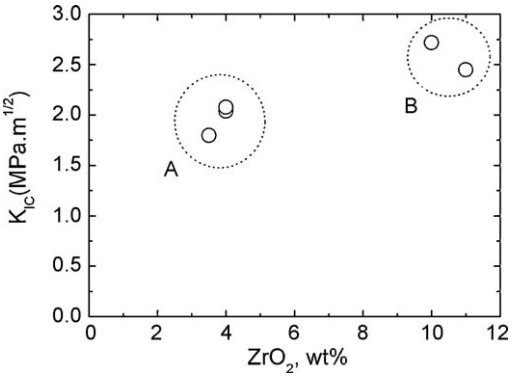

Fig. 9. Fracture toughness K_{IC} against the amount of total zirconia evaluated by the Rietveld method.

the composite. This can be attributed to the appearance of microcracks due to the presence of new zirconia grains.

In Fig. 7 the values of the flexural strength of the different composites are plotted and compared to that of a pure zircon material (Z0). The value obtained for the Z0 was 30% lower than the composite materials (ZM15–45), probably to the higher sinterization of the composite materials as seen in SEM micrographs in Figs. 3–6. The flexural strength of the composites was independent on the phase composition in the range of study. These values are slightly lower than those given in the literature for pure mullite (254 MPa) [6], pure zircon (150–320 MPa for various products fabricated at 1600 °C [8–11]) and 170 MPa for a zircon mullite composite material (mullite ≈ 14 wt%) [14]. The difference may be explained by the residual porosity, microcracks resulting from the zirconia transformation during cooling, the presence of a non-crystalline phase, and the processing condition used.

3.5. Fracture toughness (K_{IC}) and initiation fracture energy (γ_{NBT})

Many methods are currently used to measure the fracture toughness of ceramics materials. The SENB method is simple and inexpensive and has been successfully used as shown in previous reports.

At first glance the values of fracture toughness (K_{IC}) and the fracture initiation energy (γ_{NBT}) (Fig. 8) are similar to the ones found in the literature for these materials [14].

Both properties had been improved by the addition of mullite to the zircon, moreover both increased linearly with that of mullite content (wt%, M). Based on the following equations:

$$K_{IC} = 1.73 + 0.02M \quad (7)$$

$$\gamma_{NBT} = 6.20 + 0.30M \quad (8)$$

3.6. Toughening

Significant toughening can be obtained by incorporating zirconia particles (ZrO_2) in a ceramic matrix. Different mechanisms are involved in the toughening: stress-induced transformation, microcraking, crack bowing and crack deflection. In all cases, the operative toughening mechanism depends on such variables as matrix stiffness, zirconia particle size, chemical composition, temperature and strength [22–25]. For that K_{IC} is plotted against the amount of total ZrO_2 (estimated by the Rietveld method) in Fig. 9.

In the studied material microstructure the zirconia grains appeared in contact with mullite and zircon grains or surrounded only by mullite grains (see Figs. 4–6) in consequence the dissociation of the zircon grains occurred in the boundaries with mullite, and evidenced that mullite phase enhanced the dissociation of zircon. In concordance with the fact that with a higher proportion of mullite in the initial composition the contact areas between zircon and mullite grains increased.

The present study covered a wide range of zircon–mullite compositions from 15 to 45 wt% of the second phase. The addition of this second phase enhanced the zircon dissociation and gradually changed the microstructure configuration from a pure zircon material (Z0) to a zircon matrix with dispersed mullite grains (ZM15–25).

For samples with 35 wt% of mullite addition (ZM35) resulted a microstructure composed of completely interpenetrated zircon and mullite continuous phases. Further mullite addition (ZM45) caused a continuous mullite matrix with zircon and zirconia as discrete phase.

In Fig. 9, K_{IC} is plotted against the amount of total ZrO_2 wt%, formed from the zircon dissociation during the material processing. Although five different materials with different initial compositions were studied there are clearly two situations in terms of the relation between K_{IC} and the amount of ZrO_2. The zircon–mullite materials that present around 4 wt% of ZrO_2 (A, in Fig. 9), composites with a zircon matrix, have a fracture toughness around 2 MPa $m^{1/2}$ and the zircon–mullite materials with approximately 10 wt% of ZrO_2 (B, in Fig. 9), composites with a mullite matrix, have a fracture toughness around 2.5 MPa $m^{1/2}$.

4. Conclusions

Composites with different microstructures were processed from compacts of zircon containing 15–45 wt% of mullite. Sintering conditions were more effective for the production of

high density ceramics from zircon mullite mixtures than pure zircon. Zircon thermal dissociation promoted the formation of zirconia (mainly monoclinic) and silica (as glassy phase). The zirconia ($m + t$) content increased up to 11 wt% using 45% of mullite. The tetragonal ratio remained nearly constant around 7% in all the materials studied. SEM examination confirmed a progressive change of microstructure from a zircon matrix with mullite and zirconia dispersed grains to a mullite continuous phase with zircon and zirconia as discrete phases.

Due to the comparatively high density, composites showed a higher flexural strength than that of pure zircon ceramics. Reduction in the dynamic elastic modulus with the increasing amount of mullite was higher than that predicted from a mixing rule, probably due to the small residual porosity and the presence of microcracks resulting from the ZrO_2 transformation during the cooling that was enhanced by the mullite.

Fracture toughness and initiation energy increased with mullite addition from which the zirconia formation is enhanced. The induced microcracks and the increase in the contribution of the transformation toughening can promote the fracture resistance of these composites.

References

[1] Y. Shi, X. Huang, D. Yan, Fabrication of hot-pressed zircon ceramics: mechanical properties and microstructure, Ceramics International 23 (1997) 457–462.

[2] A. Everett, T. Thomas, T. Weichert, Trends in usage in glass industry, Proceedings of UNITECR, 1989, pp. 730–760.

[3] J. Mori, N. Watanbe, M. Yoshimura, Y. Oguchi, T. Kawakami, A. Matsuo, Materials design of monolithic refractories for steel ladle, Proceedings of UNITECR, 1989, pp. 541–553.

[4] L.B. Garrido, E.F. Aglietti, Zircon based ceramics by colloidal processing, Ceramics International 5 (2001) 491–499.

[5] R. Torrecillas, J. Calderon, J. Moya, M. Reece, C. Davies, C. Olagnon, G. Fantozzi, Suitability of mullite for high temperature applications, Journal of the European Ceramic Society 19 (1999) 2519–2527.

[6] M. Hamidouche, N. Bouaouadja, C. Olagnon, G. Fantozzi, Thermal shock behavior of mullite ceramic, Ceramics International 29 (2003) 599–609.

[7] H. Schneider, J. Schreuer, B. Hildmann, Structure and properties of mullite—a review, Journal of the European Ceramic Society 28 (2008) 329–344.

[8] R. Moreno, J. Moya, J. Requena, Slip casting of zircon by using an organic surfactant, Ceramics International 17 (1991) 37–40.

[9] T. Mori, H. Yamamura, H. Kobayashi, T. Mitamura, Preparation of high-purity $ZrSiO_4$ using sol–gel processing and mechanical properties of the sintered body, Journal of the American Ceramic Society 75 (9) (1990) 2420–2426.

[10] C. Veytizou, J. Quinson, Y. Jorand, Preparation of zircon bodies from amorphous precursors powders synthesized by sol–gel processing, Journal of the European Ceramic Society 22 (2002) 2901–2909.

[11] Y. Shi, X. Huang, D. Yan, TEM and SEM characterization of hot-pressed zircon ceramics, Materials Letters 23 (1995) 247–252.

[12] R. Singh, SiC fibre-reinforced zircon composites, Journal of the American Ceramic Society Bulletin 70 (1) (1991) 555–556.

[13] Y. Shi, X. Huang, D. Yan, Toughening of hot-pressed $ZrSiO_4$ ceramics by addition of y-TZP, Materials Letters 35 (3) (1998) 161–165.

[14] M. Hamidouche, N. Bouaouadja, R. Torrecillas, G. Fantozzi, Thermo-mechanical behavior of a zircon–mullite composite, Ceramics International 33 (4) (2007) 655–662.

[15] N.M. Rendtorff, L.B. Garrido, E.F. Aglietti, Effect of the addition of mullite–zirconia to the thermal shock behavior of zircon materials, Materials Science and Engineering A 498 (1–2) (2008) 208–215.

[16] D.L. Bish, J.E. Post, Quantitative mineralogical analysis using the Rietveld full-pattern fitting method, American Mineralogist 78 (1993) 932–940.

[17] H.M. Rietveld, A profile refinement method for nuclear and magnetic structures, Journal of Applied Crystallography 2 (1969) 65–71.

[18] J. Rodríguez-Carbajal, Program FullProf. 98, version 0.2, 1998.

[19] V. Pandolfelli, V. Salvini, Influence of mullitte–zirconia aggregate addition on the thermomechanical properties of high-alumina, Refractories Anales UNITECR, 1993, pp. 282–291.

[20] H. Harmuth, E. Tsechegg, Fracture mechanical characterization of ordinary ceramic refractory materials, Veitsch-Radex-Rundschau 1–2 (1994) 465–542.

[21] A. Kaiser, M. Lobert, R. Telle, Thermal stability of zircon ($ZrSiO_4$), Journal of the European Ceramic Society 28 (2008) 2199–2211.

[22] X. Jin, Martensitic transformation in zirconia containing ceramics and its applications, Current Opinion in Solid State & Materials Science 9 (6) (2005) 313–318.

[23] P.M. Kelly, L.R. Francis Rose, The martensitic transformation in ceramics—its role in transformation toughening, Progress in Materials Science 47 (5) (2002) 463–557.

[24] M. Radovic, E. Lara-Curzio, L. Riester, Comparison of different experimental techniques for determination of elastic properties of solids, Materials Science and Engineering A 368 (1–2) (2004) 56–70.

[25] N. Claussen, J. Jahn, Mechanical properties of sintered in situ-reacted mullite–zirconia composites, Journal of the American Ceramic Society 63 (3–4) (1980) 228–229.